Synthesis, Molecular Docking and Biological Evaluation of Novel 3-substituted Pyrido[2,3-*b*]pyrazine Derivatives

Madhusudhan Reddy Tammana and S. Sarveswari*
Centre for Organic and Medicinal Chemistry, VIT-Vellore, Tamil Nadu 632 014, India
*Corresponding author (e-mail: sarveswari@gmail.com; ssarveswari@vit.ac.in)

A novel series of 3-substituted pyrido[2,3-*b*]pyrazine derivatives were synthesized using Suzuki and Buchwald-Hartwig coupling reactions. All the synthesized derivatives were screened for *in-vitro* anti-inflammatory activities as inhibitors of pro-cytokines TNF-alpha and IL-6. Among them, compounds **7a**, **7b**, **7d, 9a** and **9c** showed LPS-induced TNF-α secretion of 79 ± 1.2, 98.5 ± 1.6, 95.5 ± 2.1, 92.4 ± 1.9, and 88.9 ± 1.2 pg mL^{-1} respectively at a concentration of 20 μM. Similarly, compounds **7a**, **7b** and **7d, 9a** and **9c** showed LPS-induced IL-6 secretion of 59.5 ± 2.1, 77 ± 2.1, 89 ± 2.4, 65.4 ± 2.1, and 74 ± 1.9 pg mL^{-1} respectively at a concentration of 20 μM. In addition, the compounds were tested for cytotoxic activity against A549, MCF-7, K562 & Hela cancer cell lines and all the compounds showed good biological profiles on cancer cell lines. In silico studies revealed that compounds **9a** and **9b** could bind strongly with the active site of the TNF-α protein structure and formed three hydrogen bonds with Gln61, Tyr151 amino acids with binding energies of -5.9 and -5.7 kcal/mol. Compound **9b** formed three strong hydrogen bonds with amino acids of the TGF-β protein with a binding energy of -6.0 kcal/mol. Compound **7e** bound strongly with the KRAS protein structure, making seven strong hydrogen bonds with amino acids Gly13, Val29, Asn116, Asp119, Ser145 and Ala146, each with a binding energy of -8.0 kcal/mol. Compound **7b** bound strongly with the KRAS protein structure, making four strong hydrogen bonds with amino acids Asn116, Lys117, Asp119, Ser145, each with a binding energy of -8.2 kcal/mol.

Key words: Pyrido[2,3-*b*]pyrazine; Suzuki coupling; Buchwald-Hartwig coupling; anti-inflammatory; cytotoxic activities and In-silico studies

Received: December 2020; Accepted: May 2021

The biological activity of nitrogen-containing heterocyclic compounds is well established. This makes them attractive targets for researchers for the synthesis of novel motifs.[1] Pyrazines are the most important nitrogen-containing heterocyclic compounds in biological and pharmaceutical molecules [1b, 1c]. Some pyrido pyrazine derivatives are predicted to be used to modulate the serine-threonine protein kinases function, anticancer, CHK1 inhibitor, Trypanosoma brucei inhibitor, antimalarial, GSK3β inhibitor, PDK inhibitor, and anticonvulsant activities [3]. As claimed by WHO, cancer is the second greatest cause of death universally, and is accountable for 9.6 million deaths in 2018, while 12 million deaths are projected annually by 2030. In the same way, it is becoming a major public health problem in developing countries. Cancer is the unrepressed development of anomalous cells in the human body. The growth often invades surrounding tissues and can metastasize to distant sites. To deal with different types of cancers, several treatment methods are now available. Subsequently, the invention of new anti-cancer agents has become a strategic aim worldwide [4]. But 90-95% of cancers can be affected by factors like infections, viruses, hormones, obesity, tobacco, chemicals, radiation and changes in lifestyle. Most cancers can be cured by radiology, chemotherapy and surgery[5]. Gefitinib (Anti-cancer), Tucatinib (Anti-cancer), Pazopanib Hydrochloride (Anti-cancer), and Esomeprazole Sodium (Anti-Inflammatory) are existing anti-cancer drugs currently available in the market which are nitrogen-containing heterocyclic compounds (shown in Figure 1).

Inflammation is an organism's response to infection or injury, and long-term inflammation may be caused by various long-lasting diseases such as cancer, atherosclerosis, cardiovascular diseases, neurological diseases, rheumatoid arthritis, and high fever [6-10]. Acute immune system acts as inflammatory mediators such as the cytokine receptors, chemokines leukotrienes, prostaglandins and interferons [11-12]. Among various cytokines, tumour necrosis factor-α (TNF-α) and interleukin-6 (IL-6) are the major pro-inflammatory cytokines involved in inflammatory bowel disease (IBD) [13-14]. Cytokine inhibition has become a popular research area for the development of biologically active

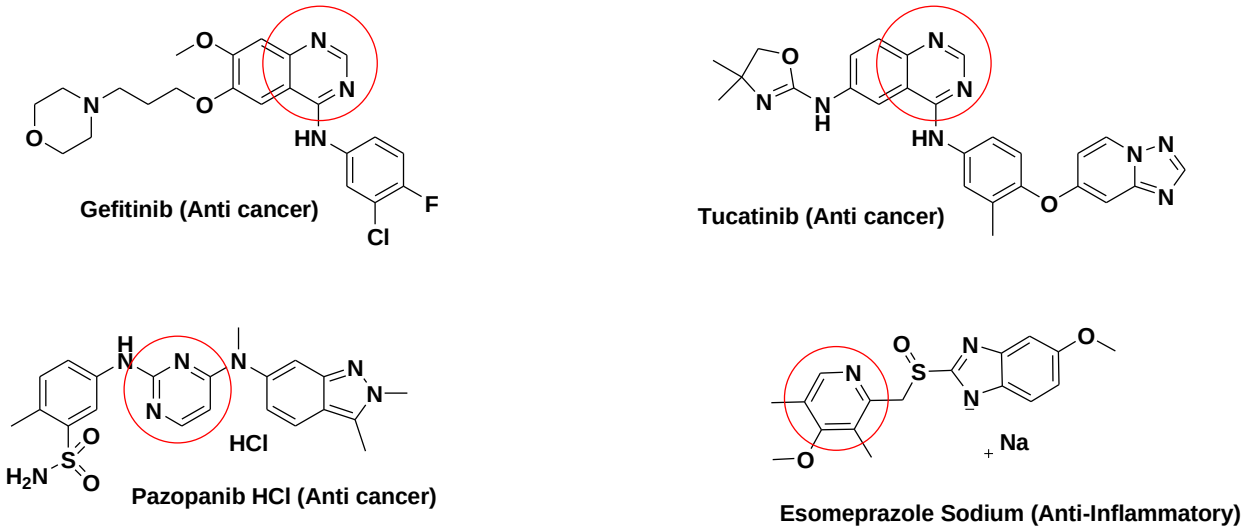

Figure 1. Biologically active nitrogen-containing heterocyclic compounds possessing pyrimidine, pyridine and quinoxaline skeletons.

molecules [15]. The TNF-α cytokine is responsible for various pathological circumstances like heart disease, diabetes, ulcerative colitis, multiple sclerosis and atherosclerosis [16-17]. IL-6 inhibitors can be used in Alzheimer's disease, psychiatric disorders, cancer, diabetes, and depression. Currently, non-steroidal anti-inflammatory drugs (NSAIDs), immune selective anti-inflammatory derivatives and TNF inhibitors are used to treat inflammation. Although drug treatment has improved to some extent, it is still a challenging task for researchers to discover the most effective and potent therapeutic agents to treat inflammation and to decrease the symptoms of acute and chronic inflammatory diseases [18]. Pyrido[2,3-*b*] pyrazine derivatives have important biological properties such as anti-cancer [19], anti-inflammation [20], anti-fungal [21], anti-bacterial [22], anti-tumor [23] etc. Several methods were developed by researchers to synthesise pyrido[2,3-b]pyrazines by condensation of an aryl-1,2-diamine with a 1,2-dicarbonyl using PEG- 400[24], Ultra sound[25], microwave[26], TBBDA/PBBS[27], RuCl-(PPh_3)$_3$-TEMPO[28], LiBr[29], MK-10[30], InCl3[31], Zn/proline[32], Ga(OTf)$_3$[33], $HClO_4$-SiO_2[34], cyclodextrins in water[35], FeMAP[36], TiO_2-P25[37], ZnO-beta zeolite[38] and silica-supported antimony(III) chloride[39] as catalysts. Because of their significant biological activity, we have focused on the development of novel pyrido[2,3-b]pyrazine derivatives and assessment of their biological activities on pro-cytokines TNF-alpha and IL-6 as anti-inflammatory inhibitors and cytotoxic activity against A549, MCF-7, K562 and Hela cancer cell lines.

RESULTS AND DISCUSSION

1. Synthetic Studies

The synthesis of pyrido[2,3-b]pyrazine derivatives is shown in **Scheme 1**. The key intermediate **5** was synthesized from the reaction of 4-methyl-3-nitropyridin-2-amine (**1)** by bromination to get compound **2** from which reduction (nitro to amine) took place to obtain compound **3**. This diamine intermediate **3** was treated with glyoxylic acid monohydrate to get cyclized compound **4,** which was chlorinated further using $POCl_3$ to get compound **5**. Compound **5** and boronic acid were screened with different palladium catalysts such as $Pd(dppf)Cl_2.CH_2Cl_2$, $Pd(OAc)_2$, $Pd(PPh_3)_4$ and $Pd(PPh_3)_2Cl_2$ with altered bases such as CS_2CO_3, Na_2CO_3, K_2CO_3 , DIPEA and TEA of 1,4 Dioxane/H_2O, Toluene/H_2O and THF/H_2O solvents. Among all, the best outcome was found with $Pd(dppf)Cl_2.CH_2Cl_2$, K_2CO_3 and 1,4 dioxane/H_2O, which afforded an 88% yield of the desired products (**7a-7e**) after 3 h in a 100°C bath. To prepare N-arylated compounds (**9a-9e**), compound **5** and amine were treated with different palladium catalysts such as $Pd_2(dba)_3$/Xantphos, $Pd_2(dba)_3$/BINAP, $Pd(OAc)_2$/ Xantphos, $Pd(OAc)_2$/XPhos and bases such as a CS_2CO_3, K_2CO_3, Na_2CO_3 and KOtBu of 1,4 Dioxane, DMF and toluene solvents. $Pd_2(dba)_3$/Xantphos, CS_2CO_3, DMF resulted in a 75% yield of desired products after 5 h in a 100°C bath. [36-39].

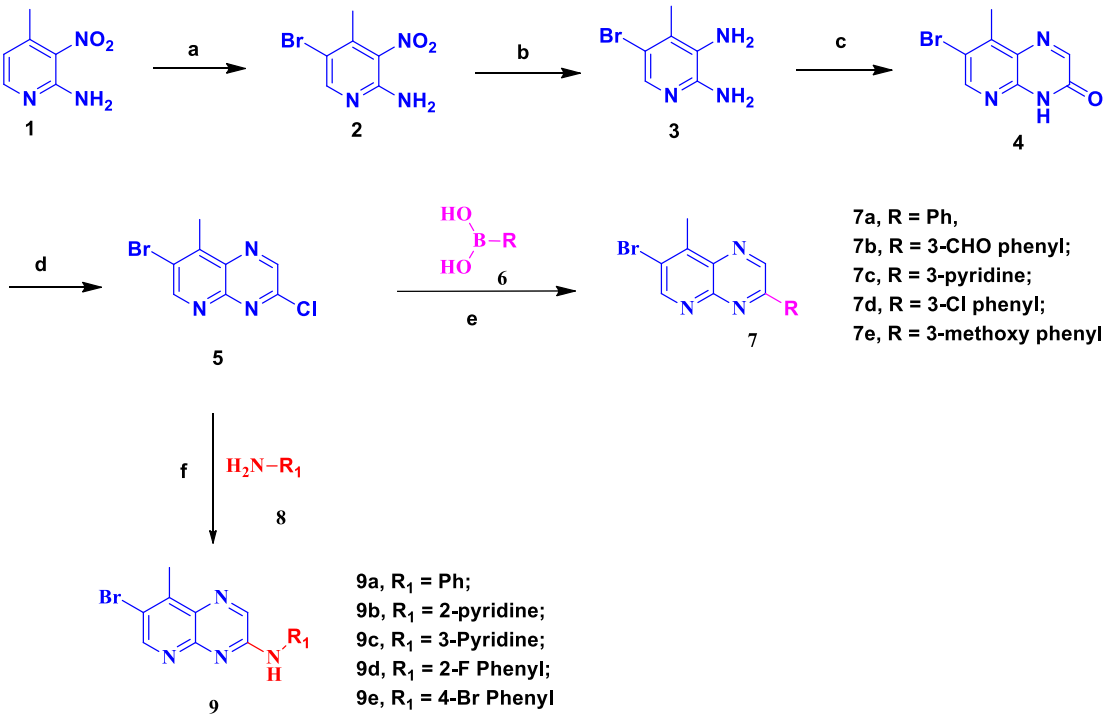

Scheme 1: Reagents and conditions: a) Br_2/AcOH, NaOAc, 10°C; b) Fe/AcOH, Con.HCl, Ethanol-Water, reflux, 3h; c) Glyoxylic acid monohydrate, 0.5 N NaOH solution, RT, 3h; d) $POCl_3$, 60°C, 2h; e) $PdCl_2(dppf)_2.CH_2Cl_2$, K_2CO_3, 1,4-dioxane and water, 100°C (Bath), 3 h; f) Pd_2dba_3, Xanphos, Cs_2CO_3, DMF, 100°C (Bath), 5 h.

Table 1. *In-Vitro* anti-inflammatory activity of test compounds **7a-7e** and **9a-7e**

A. Inhibition of TNFα pro-inflammatory cytokine

Test compound (µM)	TNFα (pg mL-1)				
	0	5	10	20	Normal
7a	303 ± 2.1	295 ± 1.7	232 ± 2.3	98.5 ± 1.6	12.4 ± 1.1
7b	309 ± 1.9	292 ± 2.1	212 ± 1.5	79 ± 1.2	13.1 ± 1.1
7c	301 ± 1.9	299 ± 1.3	298 ± 1.8	292 ± 1.9	12.2 ± 0.9
7d	403 ± 2.6	336 ± 1.8	287 ± 1.5	95.5 ± 2.1	12.9 ± 1.1
7e	309 ± 1.5	289 ± 1.6	283 ± 1.6	284 ± 1.7	12.4 ± 1.3
9a	305 ± 1.5	278 ± 1.9	201 ± 1.6	92.4 ± 1.9	12.7 ± 1.1
9b	401 ± 2.3	397 ± 2.2	394 ± 1.9	392 ± 1.7	12.5 ± 0.9
9c	302 ± 1.7	298 ± 1.7	228 ± 1.6	88.9 ± 1.2	12.5 ± 0.7
9d	309 ± 1.5	303 ± 1.4	299 ± 1.9	289 ± 1.2	12.9 ± 1.2
9e	309 ± 1.9	308 ± 2.8	302 ± 1.5	301 ± 1.8	12.8± 1.2

B. Inhibition of IL-6 pro-inflammatory cytokine

Test compound (μM)	IL-6 (pg mL-1)				
	0	5	10	20	Normal
7a	301 ± 1.9	298 ± 2.1	154 ± 2.6	77 ± 2.1	11.1 ± 1.2
7b	299 ± 2.2	281 ± 2.5	193 ± 1.9	59.5 ± 2.1	9.9 ± 0.9
7c	292 ± 1.5	289 ± 1.8	287 ± 1.9	283 ± 2.1	11.5 ± 0.8
7d	302 ± 1.3	298 ± 2.1	196 ± 2.1	89 ± 2.4	9.7 ± 0.9
7e	298 ± 2.1	297 ± 2.1	291 ± 1.9	287 ± 2.1	11.2 ± 1.2
9a	298 ± 1.2	239 ± 2.1	139 ± 2.2	65.4 ± 2.1	9.8 ± 1.1
9b	301 ± 2.1	292 ± 2.5	289 ± 2.1	282 ± 1.9	11.2 ± 0.8
9c	297 ± 1.9	273 ± 2.1	213 ± 2.2	74 ± 1.9	10.2 ± 1.2
9d	289 ± 1.7	287 ± 2.1	283 ± 2.1	280 ± 1.9	9.9 ± 1.1
9e	297 ± 1.1	252 ± 1.9	201 ± 1.9	198.3 ± 1.8	10.6 ± 1.4

2. Biological Studies

2.1. Anti-inflammatory Activity

The anti-inflammatory activity of the test compounds was analyzed by measuring the release of pro-inflammatory cytokines like TNF-α and IL-6 in RAW 264.7 cells using ELISA. The analysis demonstrated that of all the test compounds, only **7a**, **7b**, **7d, 9a**, and **9c** inhibited the secretion of LPS-stimulated cytokines (shown in Table-1). In control experiments where RAW cells were treated with only DMEM medium, the basal level of TNF-α and IL-6 secretion **7c** and **7d** were 12.2 ± 0.9 and 9.7 ± 0.9 pgmL^{-1} respectively. However, when the RAW cells were stimulated with 100 ng mL^{-1} LPS, the secretion of TNF-α and IL-6 increased to 403 ± 2.6 and 302 ± 1.3 pg mL^{-1} respectively for test compound **7d**. Interestingly when RAW cells were treated at 20 μM with test compounds **7a**, **7b**, **7d, 9a** and **9c**, the LPS induced TNF-α secretion was reduced to 98.5 ± 1.6, 79 ± 1.2, 95.5 ± 2.1, 92.4 ± 1.9, and 88.9 ± 1.2 pg mL^{-1} respectively. Similarly at 20 μM, test compounds **7a**, **7b** and **7d, 9a** and **9c** down-regulated the LPS induced IL-6 secretion to 77 ± 2.1, 59.5 ± 2.1, 89 ± 2.4, 65.4 ± 2.1, and 74 ± 1.9 pg mL^{-1} respectively.

Based on the above data, compounds **7a**, **7b**, **7d, 9a** and **9c** exhibited significant effects with pro-cytokines TNF-alpha and IL-6 cells using ELISA in RAW 264.7.

2.2. Cytotoxicity Studies

The cytotoxicity of the test compounds was assessed using MTT cell proliferation assay. The IC_{50} results exhibited by test compounds against different cancer cell lines were shown in Table-2. From the above graph, it was evident that except for compound **9c**, all the test compounds showed moderate to good cytotoxic activity against the tested cancer cell lines. In the case of A549 carcinoma cells, test compound **9d** showed promising activity, while **7e**, **9a** and **7c** showed respectable anticancer activity. Test compounds **9d**, **7d**, **7a**, **9e** and **7b** exhibited good cytotoxicity against MCF-7 cancer cells. Further, exceptional anticancer activity was observed against Hela carcinoma cells by **9a**, **9d**, **7b**, **7c** and **7d**. Test compounds **9a**, **9d** and **7d** showed good anticancer activity against K562 carcinoma cells in comparison to control cells. However, no toxicity was shown by all examined compounds against the normal HEK293 cells.

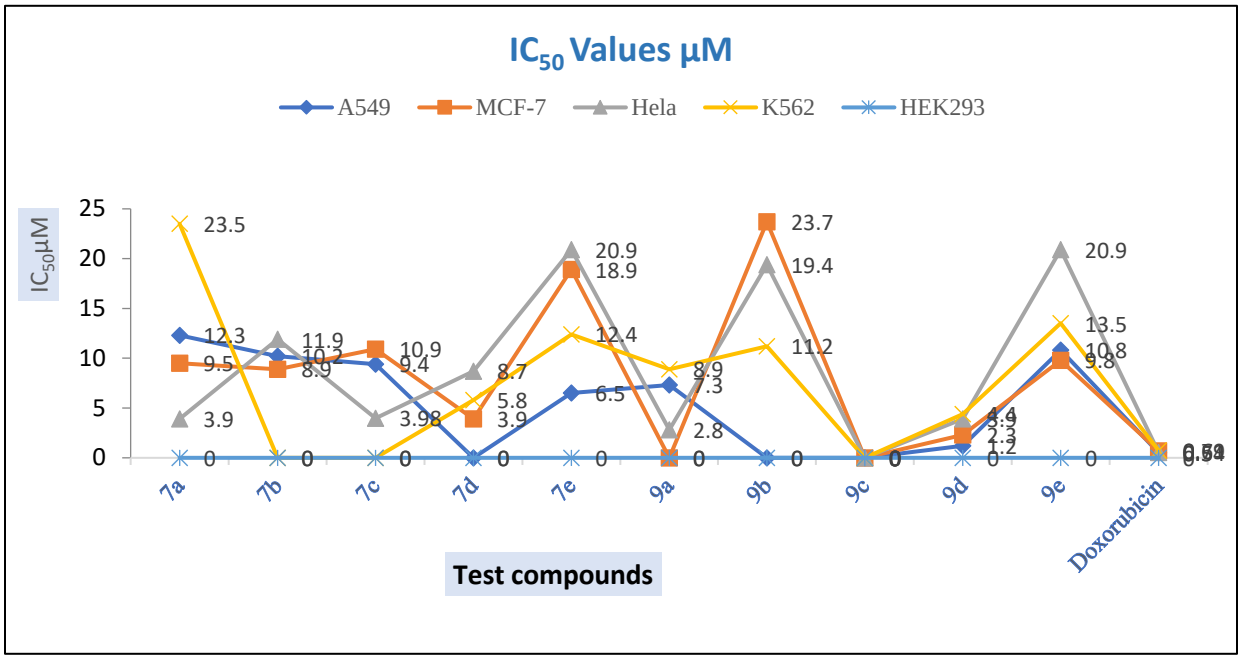

Figure 2. IC_{50} values of test compounds against different cancer cell lines.

Table 2. *In-Vitro* cytotoxic activity of test compounds **7a-7e** and **9a-9e**

Test Compound	IC_{50}µM				
	A549	MCF-7	Hela	K562	HEK293
7a	12.30 ± 1.50	9.50 ± 1.70	3.90 ± 0.90	23.50 ± 1.90	NA
7b	10.20 ± 1.20	8.90 ± 1.90	11.90 ± 1.20	NA	NA
7c	9.40 ± 0.9	10.90 ± 1.2	3.98 ± 0.80	NA	NA
7d	NA	3.90 ± 0.90	8.70 ± 0.70	5.80 ± 1.20	NA
7e	6.50 ± 1.10	18.90 ± 1.50	20.90 ± 1.20	12.40 ± 1.90	NA
9a	7.30 ± 1.20	NA	2.80 ± 0.90	8.90 ± 1.20	NA
9b	NA	23.70 ± 1.20	19.40 ± 1.60	11.20 ± 0.90	NA
9c	NA	NA	NA	NA	NA
9d	1.20 ± 0.20	2.30 ± 0.40	3.90 ± 0.90	4.40 ± 0.70	NA
9e	10.80 ± 1.20	9.80 ± 0.80	20.90 ± 1.50	13.50 ± 1.80	NA
Doxorubicin	0.50±0.20	0.69±0.50	0.54±0.30	0.71±0.45	NA

NA- No Activity
A549: Human alveolar adenocarcinoma cell line, HeLa-Human Cervical cancer cell line.
MCF-7: Human breast adenocarcinoma cell line, K562- Human chronic myelogenous leukemia cell line.
HEK 293: Human embryonic kidney cell line.
MTT: 3-(4,5-dimethylthiazol-2-yl)-2,5-diphenyltetrazolium bromide

3. In Silico Analysis

3.1. Pharmacophore Analysis

Drug-like properties of the bioactive molecules were examined based on Lipinski's Rule of 5 and Veber's Rule. The drug-like properties such as miLogP<5 represent the dissolution of test compounds in octanol/water. Poor absorption or permeation are more likely when H-bond donors >5 (expressed as the sum of all OH and NH functional groups), H-bond acceptors (expressed as the sum of all N and O groups), molecular weight >500. Substrates for biological transporters are exceptions to the rule. Veber's rule suggests that good oral bioavailability of compounds is based on properties of rotatable bonds ≤ 10, TPSA ≤140 $Å^2$ or total hydrogen bonds (acceptors plus donors) ≤ 12. However, "violation" of one rule may not result in poor absorption (shown in Table 3 & Table 4 and highlighted in green). ADME and toxicity of the phytochemicals is predicted using the admetSAR online server. The ADMET properties include parameters based on human intestinal absorption (HIA), human oral bioavailability, Caco-2 permeability, plasma protein binding, blood brain barrier penetration (BBB), acute toxicity, carcinogenicity, LD_{50} and mutagenicity.

Table 3. Pharmacophore Analysis of selected chemicals based on Lipinski Rule of 5

Ligand	miLogP	TPSA	N atoms	MW	H Donors	H Acceptors	Rotatable bonds	Volume
7a	3.84	38.68	18	300.16	3	0	1	221.42
7b	3.60	55.75	20	328.17	4	0	2	240.41
7c	2.77	51.57	18	301.15	4	0	1	217.26
7d	4.49	38.68	19	334.60	3	0	1	234.96
7e	3.34	58.90	19	316.16	4	1	1	229.44
9a	4.28	50.70	19	315.17	4	1	2	233.82
9b	3.38	63.59	19	316.16	5	1	2	229.67
9c	3.21	63.59	19	316.16	5	1	2	229.67
9d	4.40	50.70	20	333.16	4	1	2	238.75
9e	5.09	50.70	20	394.04	4	1	2	251.71

Table 4. Bioactive properties of the synthesized compounds predicted using molinspiration.

Properties	7a	7b	7c	7d	7e	9a	9b	9c	9d	9e
GPCR Ligand	-0.10	-0.09	-0.02	-0.05	0.01	0.00	0.15	0.12	-0.02	-0.01
Ion Channel modulator	0.12	0.07	0.23	0.10	0.18	0.08	0.24	0.26	-0.04	0.04
Kinase inhibitors	0.30	0.33	0.49	0.31	0.42	0.58	0.75	0.74	0.65	0.57
Nuclear receptor ligand	-0.65	-0.37	-0.66	-0.56	-0.37	-0.65	-0.70	-0.73	-0.67	-0.62
Protease inhibitor	-0.53	-0.54	-0.46	-0.53	-0.45	-0.30	-0.30	-0.19	-0.28	-0.29
Enzyme inhibitor	0.30	0.27	0.43	0.27	0.39	0.31	0.49	0.39	0.24	0.27

Table 5. Sequence similarity search and templates identification to predict 3D complex protein structures using BLASTp.

Proteins target		Templates	% of identity	E-value	Coverage
Anticancer proteins	AKT (NP_001014431.1)	4EJN_A	99.33%	0.0	92% (2-446)
		3O96_A	100%	0.0	92% (2-443)
	BCL2 (NP_000624.2)	2XA0_A	100.0%	7e-155	86% (1-207)
		5JSN_A	100.0%	2e-154	86% (1-207)
	KRAS (NP_004976.2)	2MSC_B	100.0%	6e-138	98% (1-185)
		4DSN_A	99.47%	6e-138	99% (2-188)
	p53 (BAC16799.1)	5XZC_B	99.25%	0.0	67% (92-356)
Anti-inflammatory proteins	COX2 (AAA58433.1)	6RZ3_A	99.13%	9e-172	58% (62-292)
		5F1A_A	99.82%	0.0	91% (19-570)
	NF-kB (P19838)	5IKQ_A	99.82%	0.0	91% (19-569)
		1SVC_P	99.45%	0.0	37% (2-365)
	TGF-β (NP_001020018.1)	2V2T_B	99%	0.0	37% (40-365)
		5E8V_A	98.08%	0.0	52% (262-574)
	TNF-α (P01375)	6OP0_A	99.37%	6e-115	67% (76-233)
		5MU8_A	100.0%	8e-115	67% (77-233)

Table 6. Protein structure validation of the 3D complex protein structures predicted using SAVES

Properties	Proteins	Models	ERRAT	Verify 3D	Ramachandran plot
Anti-cancer proteins	AKT	3O96_A	96.3815	83.48% (PASS)	92.8%
	BCL2	5JSN_A	99.2908	95.97% (PASS)	94.5%
	KRAS	2MSC_B	93.6416	100% (PASS)	88.0%
	P53	6RZ3	91.3649	100% (PASS)	90.2%
Anti-inflammatory Proteins	COX2	5F1A_A	96.475	91.12% (PASS)	89.5%
	NF-kB	1SVC_P	80.5369	99.04% (PASS)	85.3%
	TGF-β	5E8V_A	99.262	90.54% (PASS)	91.7%
	TNF-α	5MU8_A	85.4545	80.26% (PASS)	91.2%

3.2. Protein Structure Prediction and Modelling

Using ligand-based drug discovery, the drug likeliness analysis is performed to screen the compounds based on Lipinski's Rule of 5 and Veber's Rule. Further, one can use the target receptors to predict the protein-drug interaction based on lock and key models. The anticancer proteins and anti-inflammatory protein sequences were retrieved from NCBI and similar templates were searched using the BLASTp tool (Table 5). The best possible template sequences are used for homology modelling and protein structure validation (Table 6). Active site amino acids are identified by the CastP calculation server and the resultant protein structures are used for molecular docking against the selected chemical structures.

3.3. Molecular Docking of Anti-inflammatory Proteins

The anti-inflammatory inhibitors such as **7a-7e** and **9a-9e** lead molecules are docked with target TNF-α and TGF-β proteins to the target active site amino acids. NFKB protein structure is docked with the chemical structures and results show the **7b** structure formed 4

hydrogen bonds with Gly55, Gly69 and Lys80, with an interaction energy of -6.0 kcal/mol. **7c** and **7d** structures formed 2 hydrogen bonds with the interaction energy of -5.8 and -6.1 kcal/mol respectively within the active site regions of Gly55, Gly69 and Thr153 amino acids. COX2 protein was also docked with the selected chemical structures and showed strong interaction with the target amino acids. **9c** and **9e** showed strong interactions with COX2 protein within the active site regions of Gln203, Thr206, His207, and Tyr385 with binding energies of -8.3 and -7.8 Kcal/mol. Similarly, we also docked the TNF-α protein structure with selected chemical structures, and the results showed **9a** and **9b** formed 3 hydrogen bonds with Gln61, Tyr151 amino acids with interaction energies of -5.9 and -5.7kcal/mol. Another compound **9e** formed 2 hydrogen bonds with Gln61 and Tyr151 amino acids with an interaction energy of -6.1 Kcal/mol. Another protein TGF-β was docked with selected chemical structures and the results showed **9b** formed 3 hydrogen bonds with target receptors Ala414, Gly417, Ser432 with an interaction energy of -6.0Kcal/Mol. **9a** also strong interactions with Gly417 and Ser432 with an interaction energy of -6.1Kcal/mol. Based on overall observations, anti-inflammatory proteins interacted with the selected lead molecules and the results showed **7b**, **7c**, **7d, 7e** and **9a**, **9b** and **9e** compounds strongly interacted with NFKB, COX2, TNF-α and TGF-β proteins by forming 4, 3, and 2 hydrogen bonds (highlighted with green color in Table 7) and these compounds can potentially be synthesized and used for anti-inflammatory activity against different cancer cell lines.

Table 7. Molecular docking of anti-inflammatory proteins using AutoDock 4.2

Ligands	NF-kB		COX2		TNF-α		TGF-β	
	H-Bonds	Bond energy	H-Bonds	Bond energy	H-Bonds	Bond energy	H-Bonds	Bond energy
7a	0	-6.4	0	-8.8	0	-6.5	0	-6.8
7b	4	-6.0	1	-8.5	0	-6.4	1	-6.4
7c	2	-5.8	1	-7.5	1	-5.9	0	-6.3
7d	2	-6.1	0	-8.7	0	-6.4	0	-6.6
7e	1	-6.0	1	-8.4	0	-6.2	1	-6.7
9a	0	-6.1	1	-8.2	3	-5.9	2	-6.1
9b	0	-5.9	1	-8	3	-5.7	1	-6.0
9c	0	-5.7	2	-7.8	0	-5.6	1	-6.0
9d	0	-6.1	0	-8.6	1	-6.1	1	-6.1
9e	0	-6.0	2	-8.3	2	-6.1	1	-6.2

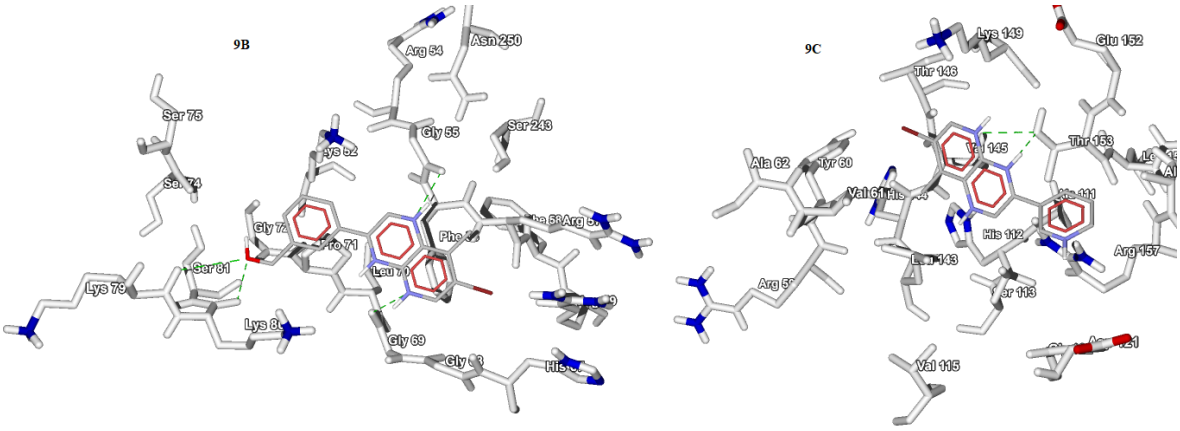

Figure 3. The docking interactions of compounds **9b** and **9c** at active site of NFKB protein

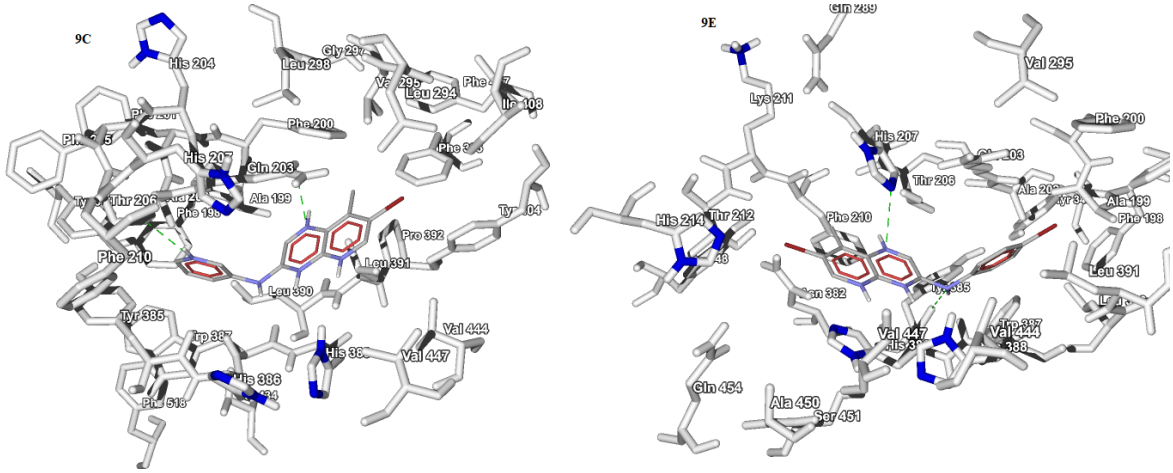

Figure 4. The docking interactions of compounds **9c** and **9e** at active site of COX2 protein.

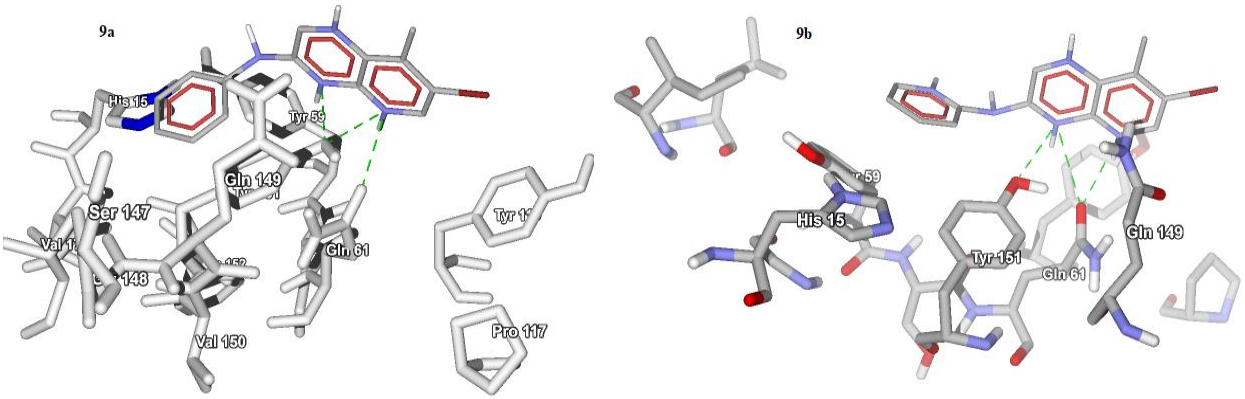

Figure 5. The docking interactions of compounds **9a** and **9b** at active site of TNF-alpha

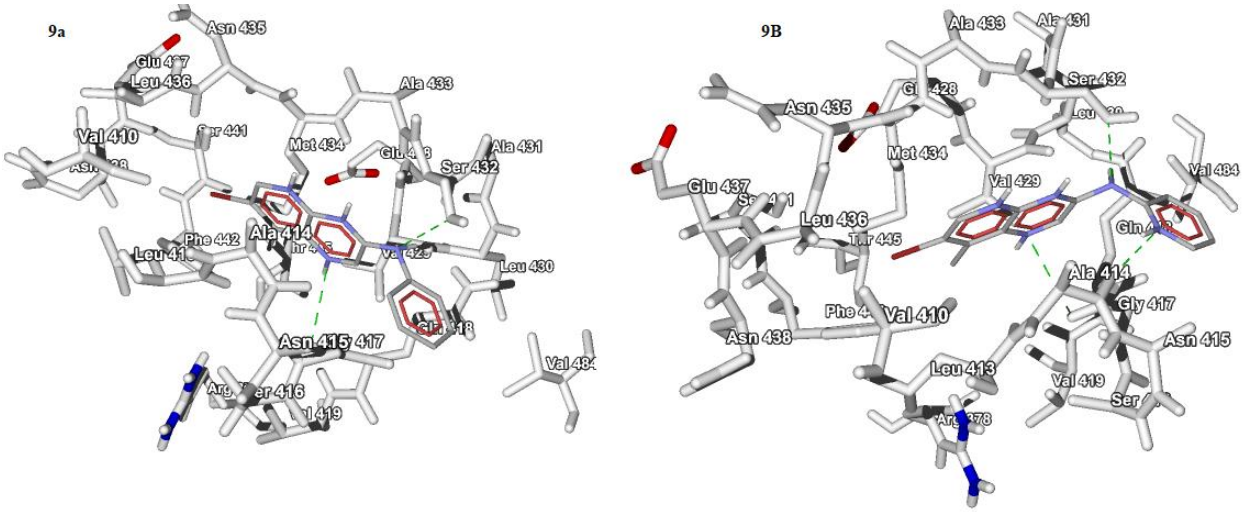

Figure 6. The docking interactions of compounds **9a** and **9b** at active site of TGF-beta protein.

3.4. Molecular Docking of Anti-cancer Proteins Using AutoDock 4.2.

The anti-cancer inhibitors such as **7a**-**7e** and **9a**-**9e** lead molecules were docked with target p53, KRAS, BCL2 and AKT proteins to the target active site amino acids. It was observed that when docking with p53 protein, **7a**, **7b**, **7c** and **7e** strongly interacted with the target receptor by forming 3 and 2 hydrogen bonds with Leu111, Phe113, His115 and Asn268 amino acids with interaction energies of -7.3, -7.1, -6.7 and -6.5Kcal/mol. Similarly, we also performed docking of BCL2 with selected ligand compounds by forming 2 hydrogen bonds for **7d** and **7e** compounds with an interaction energy of -6.1 kcal/mol bound with Tyr108 and Gly145 amino acids. We also performed docking studies with KRAS protein with selected lead molecules and the results showed **7e** had 7 hydrogen bonds with Gly13, Val29, Asn116, Asp119, Ser145, and Ala146 with a binding energy of -8.0kcal/mol, while **7b** formed 4 hydrogen bonds with Asn116, Lys117, Asp119, and Ser145 amino acids with a binding energy of -8.2 kcal/mol. **7d** and **9c** formed 2 hydrogen bonds with binding energies of -8.2 and -7.4 kcal/mol respectively with active sites of Gly13, Val29 and Asn116 amino acids. We also screened the chemical structures with AKT protein, and the results showed **7d** and **7e** compounds showed 2 hydrogen bonds bound with Ser205, Thr211 and Lys268 amino acids with an interaction energy of -9.0 Kcal/mol. Based on overall observation, anticancer proteins interacted with selected lead molecules and the results showed **7a**, **7b**, **7d**, **7e** and **9c** compounds strongly interacted with p53, BCL2, KRAS and AKT proteins by forming 7, 4, 3, and 2 hydrogen bonds (highlighted with green color in Table 8) and these compounds can potentially be synthesized and used for anti-cancer activity against different cancer cell lines.

Table 8. Molecular docking of anti-cancer proteins using AutoDock 4.2

Ligands	AKT		BCL2		KRAS		p53	
	H-Bonds	Bond energy	H-Bonds	Bond energy	H-Bonds	Bond energy	H-Bonds	Bond energy
7a	0	-9.2	0	-6.4	0	-7.6	2	-6.7
7b	1	-9.1	1	-6.2	4	-8.2	2	-7.3
7c	1	-8.4	1	-5.8	0	-7.1	2	-6.5
7d	2	-9	2	-6.1	2	-8.2	1	-7.1
7e	2	-9	2	-6.1	7	-8	2	-7.1
9a	0	-8.9	0	-5.9	1	-8	0	-6.7
9b	1	-8.5	0	-5.9	1	-7.6	0	-6.6
9c	1	-8.1	0	-5.6	2	-7.4	1	-6.6
9d	0	-8.8	0	-6.5	1	-8.3	0	-7
9e	0	-8.5	0	-6.2	0	-7.4	1	-6.3

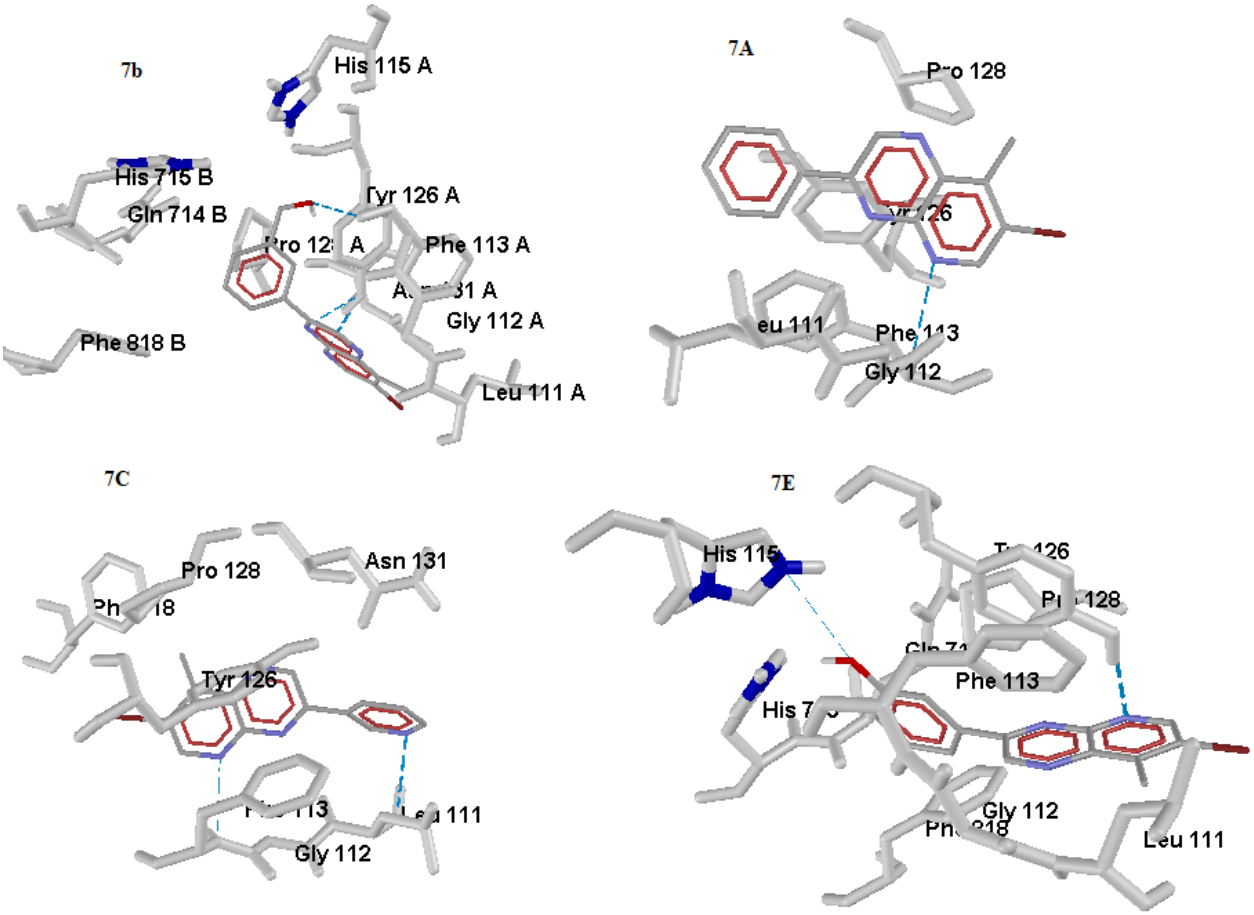

Figure 7. The docking interactions of compounds **7a, 7b, 7c** and **7e** at active site of p53 protein.

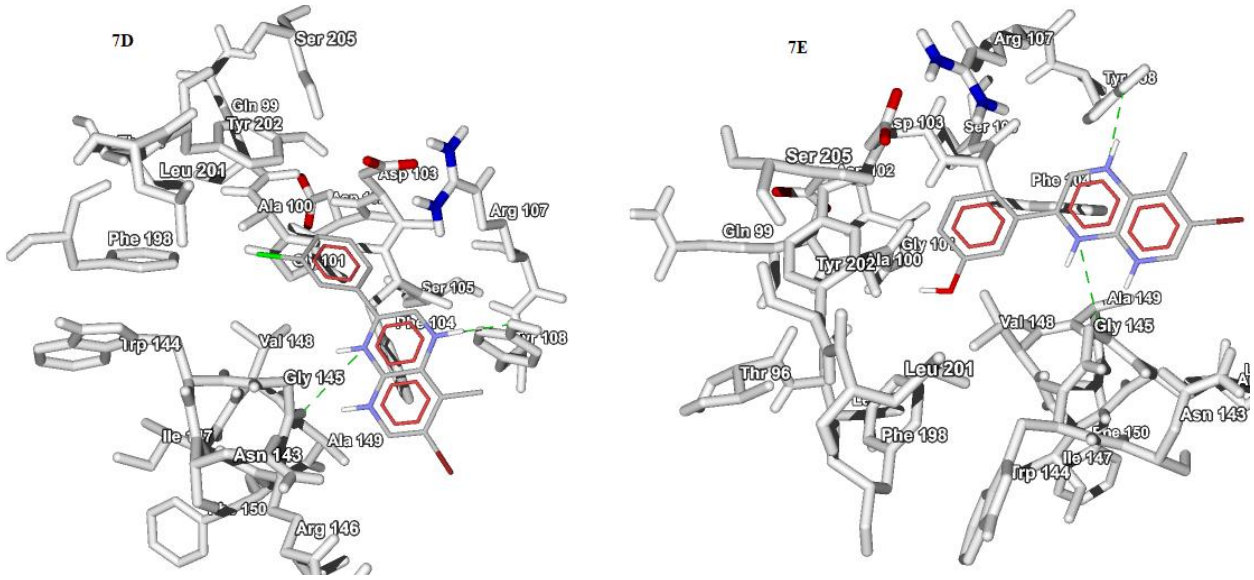

Figure 8: The docking interactions of compounds **7d** and **7e** at active site of BCL2 protein.

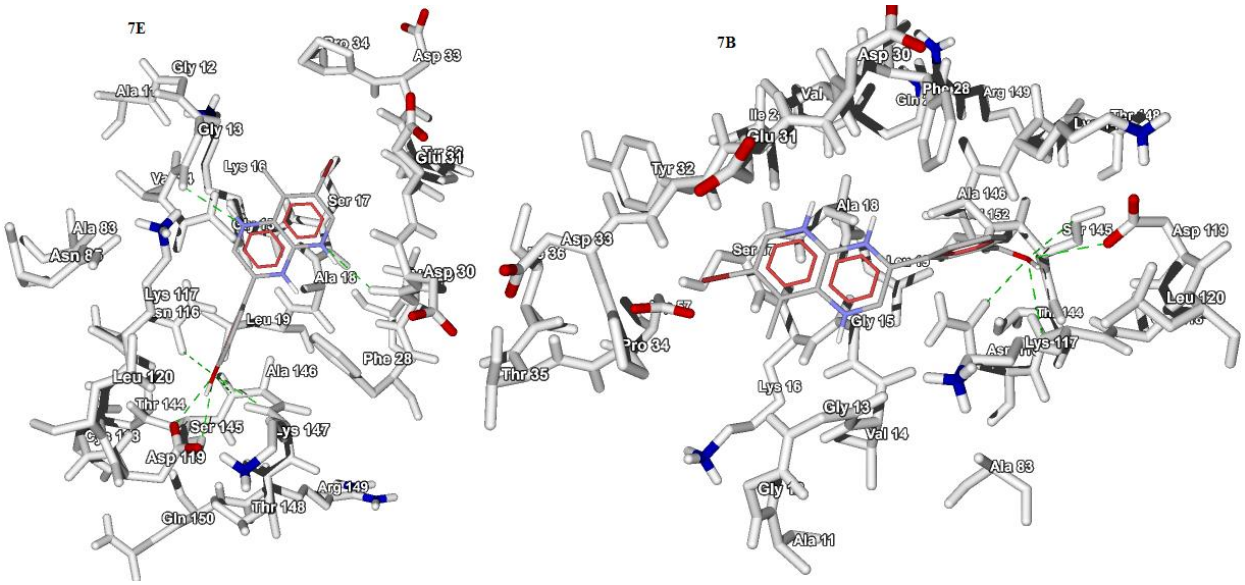

Figure 9. The docking interactions of compounds **7e** and **7b** at active site of KRAS protein

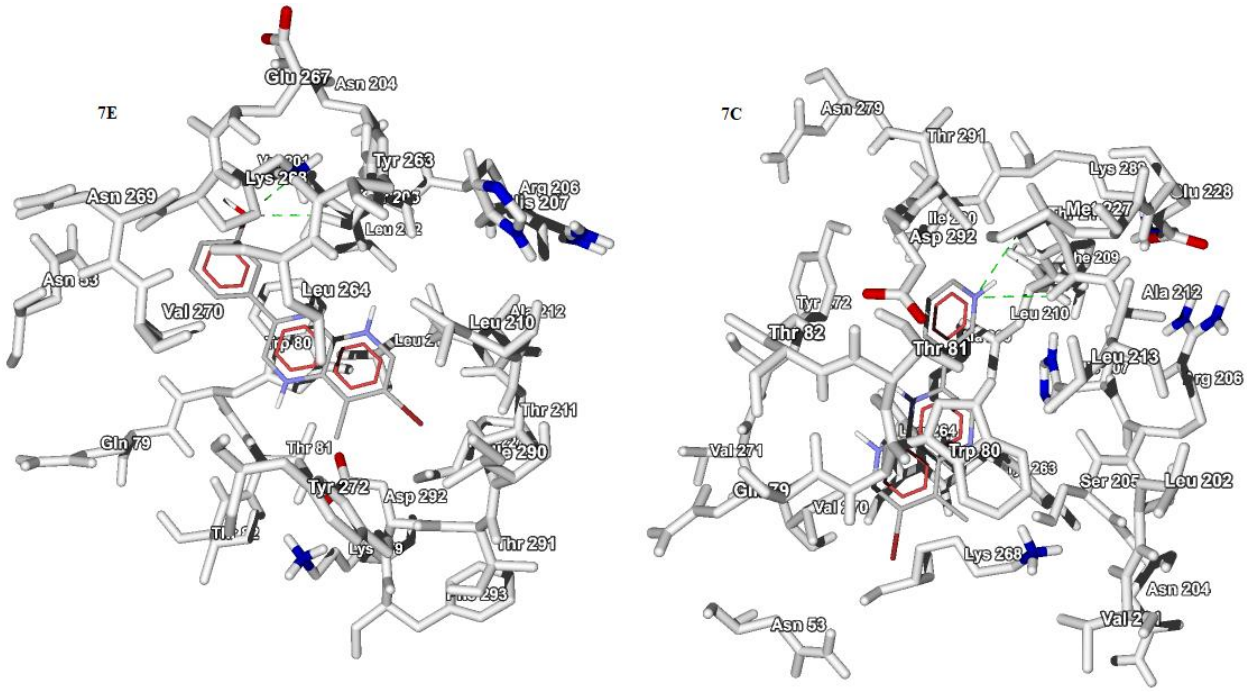

Figure 10. The docking interactions of compounds **7e** and **7c** at active site of AKT protein

CONCLUSION

In summary, we have demonstrated that the 3-substituted 7-bromo8-methyl pyrido[2,3-b] pyrazine scaffold underwent sequential synthesis using Suzuki [**7a-7e**] and Buchwald-Hartwig coupling reactions [**9a-9e**]. In this examination we found that all test compounds exhibited remarkable toxicity towards all cell lines i.e. A549 (lung), MCF-7 (breast), Hela (cervical), K562 (leukemia), and HEK293 (kidney) and interestingly compound **9d** showed comparable toxicity (IC_{50} = 1.2 - 4.4µM) to that of the reference drug Doxorubicin (IC_{50} = 0.50 – 0.71µM). In the anti-inflammatory study, test compounds **7a**, **7b**, **7d, 9a** and **9c** exhibited significant effect with pro-cytokines TNF-alpha and IL-6 cells using ELISA in RAW 264.7. Similarly, docking studies revealed that **7b**, **7e** and **9a** showed good kinase inhibitory effects and enzyme inhibitory effects. Compounds **7b**, **7e** and **9a** had strong interactions with anti-cancer and anti-inflammatory

proteins and may be used as potential drug compounds for their anti-apoptosis properties. In summary, 3-substituted pyrido[2,3-b] pyrazine derivatives can be regarded as promising candidates for the development of new anti-cancer and anti-inflammatory drugs.

EXPERIMENTAL PROCEDURE

All reactions were examined by TLC using pre-coated silica gel plates with n-hexane and ethyl acetate as the mobile phase and on TLC plates spot visualization was done by UV illumination. ^{1}H NMR and ^{13}C NMR were analyzed using Bruker 400 MHz with TMS as an internal reference. High resolution mass spectra were recorded on a Bruker MaXis HR-MS (ESI-Q-TOF-MS) instrument. All the reagents were procured from Sigma Aldrich and used as received. Column chromatography was performed with silica gel of 230-400 mesh size for all purifications. Melting points (m.p.) were recorded in open capillary tubes using an Elchem microprocessor based DT apparatus.

5-bromo-4-methyl-3-nitropyridin-2-amine (**2**) Yellow solid, Yield: 90 %, m.p.: 160-162 °C; ^{1}H NMR (400 MHz, $CDCl_3$): δ ppm 8.28 (s, 1H), 7.06 (s, 2H), 2.31 (s, 3H),^{13}C NMR (100 MHz, $CDCl_3$): δ ppm 152.64, 151.53, 141.56, 132.56, 108.62, 19.29.

5-bromo-4-methylpyridine-2, 3-diamine (**3**) Brown solid, Yield: 81%, m.p.: 161-163°C, ^{1}H NMR (400 MHz, $CDCl_3$): δ ppm 7.37 (s, 1H), 5.52 (s, 2H), 4.77 (s, 2H), 2.12 (s, 3H). ^{13}C NMR (100MHz, $CDCl_3$): δ ppm 147.42, 135.28, 129.68, 124.88, 111.25, 16.93.

7-bromo-8-methylpyrido[2,3-b] pyrazin-3-ol (**4**) Brown solid, Yield: 84 %, m.p.:242-244 °C;^{1}H NMR (400 MHz, $CDCl_3$): δ ppm 12.22 (s, 1H), 8.62 (s, 1H), 8.41 (s, 2H), 2.54 (s, 3H), ^{13}C NMR (100MHz, $CDCl_3$): δ ppm 155.71, 151.5, 146.28, 124.41, 17.01.

7-bromo-3-chloro-8-methylpyrido[2,3-b]pyrazine (**5**) Colorless solid , Yield: 55 %, m.p.: 153-155°C;^{1}H NMR (400 MHz, $CDCl_3$): δ ppm 9.07 (s, 1H), 8.90 (s, 1H), 2.81 (s, 3H). ^{13}CNMR (100MHz, $CDCl_3$): δ ppm 154.31, 147.22, 146.86, 146.58, 146.43, 136.44, 123.62, 15.81.

1. General procedure for the synthesis of pyrido[2,3-b]pyrazine annulated heterocycles by Suzuki coupling (7a-7e)

A mixture of compound **5** (200 mg, 0.773 mmol), aryl boronic acid (140 mg, 0.933 mmol) and K_2CO_3 (213 mg, 1.54 mmol) were added under nitrogen atmosphere into a mixture of 1,4-dioxane (3 mL) and water (1 mL), followed by Pd(dppf)$Cl_2CH_2Cl_2$ (28 mg, 0.05 mmol). The reaction was carried out at reflux temperature, and the completion of the reaction was monitored by TLC. The reaction mixture was filtered through cellite powder, washed with ethyl acetate (10 mL), and then diluted with ethyl acetate (50 mL) and water (15 mL). After separating the layers, the organic layer was washed with brine solution, dried over Na_2SO_4, and concentrated under vacuum. This crude product was purified by column chromatography using ethyl acetate and n-hexane (7:3 v/v) to obtain compounds **7a-7e.**

7-bromo-8-methyl-3-phenylpyrido[2,3-b]pyrazine (**7a**) Colorless solid, Yield: 88 %, m.p.: 148-150 °C; ^{1}H NMR (400 MHz, $CDCl_3$): δ ppm 9.53 (s, 1H), 9.10 (s, 1H), 8.25 (t, *J* = 1.60 Hz, 2H), 7.58 (d, *J* = 7.20 Hz, 3H), 2.98 (s, 3H).^{13}CNMR (100MHz, $CDCl_3$): δ ppm 154.67, 151.90, 148.73, 148.00, 145.48, 137.38, 135.73, 130.91, 129.29, 127.69, 123.71, 16.72. HRMS-ESI (m/z) calcd for $C_{14}H_{11}BrN_3$ $[M+H]^+$= 300.0136, found = 300.0149.

3-(7-bromo-8-methylpyrido[2,3-b]pyrazin-3-yl)benzaldehyde (**7b**) Brown solid, Yield:68 %, m.p.: 213-215°C; ^{1}H NMR (400 MHz, $CDCl_3$): δ ppm 9.60 (s, 1H), 9.15 (s, 1H), 8.76 (s, 1H), 8.55 (d, *J* = 7.60 Hz, 1H), 8.08 (d, *J* = 7.60 Hz, 1H), 7.79 (t, *J* = 7.60 Hz, 1H), 3.01 (s, 3H). ^{13}CNMR (100MHz, $CDCl_3$): δ ppm 191.62, 155.33, 150.52, 148.91, 148.14, 145.12, 137.38, 137.25, 136.76, 133.24, 131.81, 130.11, 128.58, 124.06, 16.81. HRMS-ESI (m/z) calcd for $C_{15}H_{11}BrN_3O$ $[M+H]^+$= 328.0085, found = 328.0093.

7-bromo-8-methyl-3-(pyridin-3-yl)pyrido[2,3-b]pyrazine (**7c**) Brown solid, Yield: 90%, m.p.: 240-242 °C; ^{1}H NMR (400 MHz, $CDCl_3$): δ ppm 9.60 (s, 1H), 9.15 (s, 1H), 8.75 (s, 1H), 8.54 (d, *J* = 7.60 Hz, 1H), 8.08 (d, *J* = 7.60 Hz, 1H), 7.79 (t, *J* = 7.60 Hz, 1H), 3.01 (s, 3H). ^{13}CNMR (100MHz, $CDCl_3$): δ ppm 159.87, 156.14, 155.72, 149.10, 148.29, 147.21, 144.36, 137.64, 129.44, 124.48, 16.79. HRMS-ESI(m/z) calcd. for $C_{13}H_{10}BrN_4$ $[M+H]^+$= 301.0089, found = 302.0049.

7-bromo-3-(3-chlorophenyl)-8-methylpyrido[2,3-b]pyrazine (**7d**) Brown solid, Yield: 80%, m.p.: 158-160 °C;^{1}H NMR (400 MHz, $CDCl_3$): δ ppm 9.49 (s, 1H), 9.12 (s, 1H), 8.24 (s, 1H), 8.10 (q, *J* =4 Hz, 1H), 7.53-7.52 (m, *J* = 4 Hz, 2H), 2.98 (s, 3H). ^{13}CNMR (100MHz, $CDCl_3$): δ ppm 155.17, 150.42, 148.84, 148.09. 145.12, 137.43, 137.30, 135.51, 130.87, 130.51, 127.75, 125.63, 123.95, 16.77. HRMS-ESI *(m/z)* calcd. for $C_{14}H_{10}BrClN_3$ $[M+H]^+$= 333.9747, found = 333.9754.

7-bromo-3-(3-methoxyphenyl)-8-methylpyrido[2,3-b]pyrazine (**7e**) Brown solid, Yield: 70%, m.p.: 176-178 °C; ^{1}H NMR(400 MHz, $CDCl_3$): δ ppm 9.48 (s, 1H), 9.09 (s, 1H), 7.77 (d, *J* = 6.80 Hz, 2H), 7.47 (t, *J* = 8.40 Hz, 1H), 7.07 (t, *J* = 7.20 Hz, 1H), 3.93 (s, 3H), 2.96 (s, 3H). ^{13}CNMR (100MHz, $CDCl_3$): δ ppm 160.32, 154.67, 151.58, 148.76, 147.95, 145.51, 137.27, 137.03, 130.31, 123.69, 119.98, 116.39, 113.16, 55.46, 16.70.

HRMS-ESI (m/z) calcd. for $C_{15}H_{13}BrN_3O[M+H]^+$= 329.0242, found = 330.0253.

2. General procedure for the synthesis of pyrido[2,3-*b*]pyrazine annulated heterocycles by Buchwald coupling reaction (9a-9e)

A mixture of compound **5** (200 mg, 0.775 mmol), aryl amine (79.4 mg, 0.851 mmol) and CS_2CO_3 (504 mg, 1.54 mmol) were added into DMF (4 mL). The reaction mixture was purged with N_2 for 10 min, subsequently $Pd_2(dba)_3$ (35 mg, 0.038 mmol) and Xanphos (18 mg, 0.038 mmol) were added, and the reaction was carried out under a nitrogen atmosphere with stirring at 100°C for 5 h. After completion of reaction (monitored by TLC), the entire reaction mixture was filtered through a cellite bed, washed with ethyl acetate (10 mL), and then diluted with ethyl acetate (50 mL) and water (15 mL). The separated organic layer was washed with brine, dried over Na_2SO_4, and concentrated under vacuum. This residue was purified by column chromatography using ethyl acetate and n-hexane (6:4 v/v) to obtain the compounds **9a**-**9e**.

7-bromo-8-methyl-N-phenylpyrido[2,3-b]pyrazin-3-amine (**9a**) Brown solid, Yield: 80%, m.p.:260-262 °C;^{1}H NMR (400 MHz, $CDCl_3$): δ ppm 9.07 (s, 1H), 7.48 (d, *J* = 9.60 Hz, 2H), 6.72 (d, *J* = 8.00 Hz, 2H), 6.19-6.17 (m, 2H), 5.85-5.84 (m, 1H), 1.48 (s, 3H).^{13}CNMR (100MHz, $CDCl_3$): δ ppm 154.47, 150.34, 148.81, 144.97, 141.17, 134.14, 127.91, 127.87, 123.90, 21.89**.** HRMS-ESI (m/z) calcd. for $C_{14}H_{12}BrN_4$ $[M+H]^+$= 315.0245, found = 315.0247.

7-bromo-8-methyl-N-(pyridin-2-yl)pyrido[2,3-b]pyrazin-3-amine (**9b**) Yellow solid, Yield: 60%, m.p.: 230-232 °C; ^{1}H NMR (400 MHz, DMSO-d_6): δ ppm 10.82 (s, 1H), 9.08 (s, 1H), 8.79 (d, *J* = 2.40 Hz, 1H), 8.49 (d, *J* = 5.70 Hz, 1H), 8.37 (t, *J* = 2.00 Hz, 1H), 7.86 (d, *J* = 5.70 Hz, 1H), 7.08 (t, *J* = 5.70 Hz, 1H), 2.80 (s, 3H).^{13}CNMR (100MHz, DMSO-*d6*): δ ppm152.97, 149.35, 149.02, 148.67, 148.87, 144.54, 143.89, 138.80, 136.09, 123.22, 118.97, 112.96, 17.21. HRMS-ESI (m/z) calcd.for $C_{13}H_{11}BrN_5$ $[M+H]^+$= 316,0198 found = 316.0204.

7-bromo-8-methyl-N-(pyridin-3-yl)pyrido[2,3-b]pyrazin-3-amine (**9c**)Yellow solid, Yield: 60%, m.p.: 276-278°C;^{1}H NMR (400 MHz, DMSO-d_6): δ ppm 10.52 (s, 1H), 9.08 (d, *J* = 3.30 Hz, 1H), 8.78 (s, 1H), 8.74 (s, 1H), 8.42-8.39 (m, 1H), 8.28 (d, *J* = 3.30 Hz, 1H), 7.45 (dd, *J* = 3.30 Hz, 8.20 Hz, 1H), 2.74 (s, 3H). ^{13}CNMR (100MHz, DMSO-d_6): δ ppm 149.52, 148.74, 145.68, 144.18, 143.58, 143.49, 140.92, 137.03, 136.24, 125.48, 123.79, 123.19, 17.14. HRMS-ESI (m/z) calcd. for $C_{13}H_{11}BrN_5$ $[M+H]^+$= 316.0198, found = 315.9937.

7-bromo-N-(2-fluorophenyl)-8-methylpyrido[2,3-b]pyrazin-3-amine (**9d**) Brown solid, Yield: 50%, m.p.: 258-260 °C;^{1}H NMR (400 MHz, DMSO-d_6): δ ppm 9.80 (s, 1H), 9.01 (s, 1H), 8.73-8.68 (m, 2H), 7.24-7.08 (m, 3H), 2.75 (s, 3H). ^{13}CNMR (100MHz, DMSO-*d6*): δ ppm 154.59, 149.66, 148.71, 145.74, 144.39, 143.67, 136.24, 127.82, 127.71, 124.38, 123.66, 121.74, 115.36, 16.94. HRMS-ESI (m/z) calcd. for $C_{14}H_{11}BrFN_4$ $[M+H]^+$= 333.0151, found = 333.0160.

7-bromo-N-(4-bromophenyl)-8-methylpyrido[2,3-b]pyrazin-3-amine **(9e)** Brown solid, Yield: 70%, m.p.: 242-244 °C; ^{1}H NMR (400 MHz, $CDCl_3$): δ ppm 9.53 (s, 1H), 7.86 (s, 1H), 7.80 (s, 1H), 7.01 (d, *J* = 8.80 Hz, 2H), 6.67 (d, *J* = 8.80 Hz, 2H), 1.81 (s, 3H). ^{13}C NMR (100 MHz, DMSO): δ ppm 149.58, 148.57, 145.63, 144.15, 144.11, 139.72, 136.29, 132.07, 131.76, 128.88, 128.76, 123.15, 121.13, 17.21, HRMS-ESI(m/z) calcd. for $C_{14}H_{11}Br_2N_4$ $[M+H]^+$= 392.9350, found = 392.9350.

3. Cytotoxicity Studies

3.1. Cytotoxicity Assay

The *in vitro* cytotoxicity was assessed using the 3-(4,5-dimethylthiazol-2yl)-2,5-diphenyl tetrazolium bromide (MTT) staining method. The assay is based on the spectrophotometric measurement of the mitochondrial reduction of MTT salt by dehydrogenases of viable cells. The MTT salt is reduced and converted to insoluble purple formazan crystals by viable cells which are measured at 570 nm. The cell lines used in the study include: A549- Human alveolar adenocarcinoma cell line, Hela - Human Cervical cancer cell line, MCF-7 - Human breast adenocarcinoma cell line, K562 - Human chronic myelogenous leukemia cell line and HEK 293 - Human embryonic kidney cell lines. Cells were incubated at a density of 5×10^3 cells well^{-1} in 96-well plates for 12 h. Further, the cells were treated with various concentrations of test compounds (1–200 μM). The cells were incubated at 37 °C for 48 h and then 20 μl of MTT solution (5 mg ml^{-1} in PBS) was added to each well and further incubated for an additional 4h at 37 °C. The purple-coloured formazan crystals formed were dissolved in 150 μl well^{-1} of DMSO and the cell proliferation (%) was measured at 570 nm in a microplate reader (BioRad Laboratories, Hercules, CA, USA). The results are represented as the means of triplicate experiments run in four replicates. The IC_{50} values (inhibitory concentration 50%) for all tested drugs in all cell lines were estimated from the log concentration–effect curves in Graph Pad Prism (GraphPad software Inc., CA, USA) using non-linear regression analysis.

3.2. Anti-inflammatory activity

The anti-inflammatory activity of test compounds was determined using a sandwich ELISA assay. The quantification of pro-inflammatory cytokines TNF-α and IL-6 secreted from RAW 264.7 macrophages was determined using an enzyme-linked immune sorbent assay kit (Biosource International, USA). Initially, RAW 264.7 macrophages were cultured in 90 mm culture dishes at a density of 5×10^6 cells well^{-1} for 12 h. Then the RAW 264.7 cells were pre-treated with test compounds at concentrations 5, 10 and 20 μM and incubated for 2 h. Then the RAW macrophages were stimulated with LPS (100 ng ml^{-1}). After the respective treatments, the cells were incubated for 24h at 37 °C. Further, the culture supernatant was collected and the release of TNF-α and IL-6 into the culture supernatant was quantitatively measured using the enzyme-linked immunoassay.

4. Computational Screening and Molecular Docking

4.1. Pharmacophore and Bioactive properties

The drug-like properties of the bioactive molecules were examined based on Lipinski's Rule of 5 and Veber's Rule, and predicted using Molinspiration software (https://www.molinspiration.com). The drug-like properties such as miLogP<5 represent the dissolution of compounds in octanol/water. The properties of poor absorption or permeation are more likely when H-bond donors >5 (expressed as the sum of all OH and NH functional groups), and H-bond acceptors (expressed as the sum of all N and O groups), molecular weight >500. Substrates for biological transporters are exceptions to the rule. Veber's rule suggests good oral bioavailability of compounds based on properties of rotatable bonds ≤ 10, TPSA ≤140 Å^2 or total hydrogen bonds (acceptors plus donors) ≤ 12. However, "violation" of one rule may not result in poor absorption.

5. ADMET Properties

ADME and toxicity of phytochemicals was predicted using the admetSAR online server (http://lmmd.ecust.edu.cn/admetsar1/). The ADMET properties consider the parameters of atoms based on human intestinal absorption (HIA), human oral bioavailability, Caco-2 permeability, plasma protein binding, blood brain barrier penetration (BBB), acute toxicity, carcinogenicity, LD_{50}. Mutagenicity is considered for the most active molecules and screened experimentally using molecular docking.

6. Protein Structure Prediction and Modeling

The anti-cancer and anti-inflammatory proteins were retrieved from the NCBI database. The anti-cancer target proteins such as AKT, BCL2, KRAS, p53 proteins and anti-inflammatory proteins COX2, NFKB, TGFB and TNF-α proteins were the best targets for the protein-ligand interactions. The BLASTp tool was used to predict the protein templates and for homology modelling to predict the 3D complex protein structure using MODELLERv9.25 and Swiss PDB viewer software. The stereochemical activity of the atom-to-atom interactions was predicted using the Structure Analysis and Validation Server (SAVES: https://saves.mbi.ucla.edu/). Active sites and ligand binding site amino acids were predicted using CastP calculation server. The best modelled protein structures were used for molecular docking.

7. Molecular Docking and Virtual Screening

Molecular docking of anti-cancer and anti-inflammatory proteins plays a vital role in drug discovery. The best active sites and ligand binding sites were predicted and targeted for docking using Autodock4.2 and AutoDock Vina (http://autodock.scripps.edu/) and the interaction energies were calculated based on the number of hydrogen bonds, binding amino acids and the binding energies to the target amino acids. The protein structure was selected to add Gasteiger chargers and hydrogen atoms to the polar group of amino acids in the macromolecule, whereas ligand structure by adding torsion counts of amide bonds rotatable and all active bonds non-rotatable and generated the PDBQT file for both protein and ligand structures. AutoDock was used to dock proteins and ligand structures by adding Lamarckian genetic algorithm (LGA) with default parameters. The best docking conformation for protein-ligand interactions was predicted with the energy value in kcal/mol and followed by the analysis of hydrogen bonding interactions and hydrophobic interactions. The best docking complex for protein-ligand was screened based on clustering analysis and visualized using Pymol (https://pymol.org/2/) and BIOVIA Discovery Studio (2017V).

ACKNOWLEDGEMENTS

The authors would like to thank the administration of VIT University, Vellore, India, which provided the facilities to carry out this research work, as well as SIF-Chemistry for providing the NMR facility. Authors are grateful to IIT Madras for the HRMS facility. Authors are also thankful to the School of Life Sciences, University of Hyderabad for providing biological

studies and also to the Department of Biotechnology, School of Applied sciences, REVA university for supporting the docking study.

SUPPLEMENTARY DATA

Supplementary data associated with this article can be found via the "Supplementary Content" section.

REFERENCES

1. (a) Argyros, O., Lougiakis, N., Kouvari, E., Papafotika, A., Raptopoulou, C. P., Psycharis, V., Christoforidis, S., Pouli, N., Marakakos, P. and Tamvakopoulos, C. (2017) Design and synthesis of novel 7-aminosubstituted pyrido[2,3-*b*] pyrazines exhibiting anti-breast cancer activity. *E. J. Med. Che*., **126**, 954-968; (b) Gangarapu, N. R., Ranganatham, A., Reddy, E. K., Surendra H. D., Sajith, A. M., Yellappa, S. and Chandrasekhar, K. B. (2019) Design, Synthesis and Biological Evaluation of 3,5-disubstituted 2-Pyrazineamide derivatives as Antitubercular agents. *J. Heterocycl. Chem.,* **56**, 1117-1126; c) Gangarapu, N. R., Ranganatham, A., Reddy, E. K., Yellappa, S., Chandrasekhar, K. B. (2020) 2-Aminoaryl-3,5-diaryl pyrazines: Synthesis, biological evaluation against Mycobacterium tuberculosis and docking studies. *Arch. Pharm.,* **353(7)**, 1900368.

2. a) WO2014/106763 A1. b) Orestis Argyros., Nikolaos Lougiakis and Eva Kouvari (2017) Design and synthesis of novel amino substituted pyrido[2,3-b]pyrazines exhibiting anti-breast cancer activity. *Eur. J. Med. Chem*., **126**, 954-968; (c) Auberson, Y. P., Bischoff, S., Moretti, R., Schmutz, M. and Veenstra, S. J. (1998) 5-Aminomethylquinoxaline-2,3-diones. Part I: A Novel Class of AMPA receptor Antagonists. *Bioorg. Med. Chem. Lett*., **8(1)**, 65-70, (d) Reynolds, R. C., Johnson, C. A., Piper, J. R. and Sirotnak, F. M. (2001) Synthesis and antifolate evaluation of the aminopterin analogue with a bicyclo[2.2.2]octane ring in place of the benzene ring. *Eur. J. Med. Chem*., **36**, 237-242.

3. (a) Stoffels, K., Mathys, V., Fauville-Dufaux, M., Wintjens, R. and Bifani, P. (2012) Antimicrob Systematic Analysis of Pyrazinamide-Resistant Spontaneous Mutants and Clinical Isolates of Mycobacterium tuberculosis. *Antimicrobial Agents and Chemother.* **56(10)**, 5186 - 5193; (b) Humphrey, J., Kablaoui, N., Kazmirski, S., Kraus, M., Kupchinsky, S., John, J. L., Lingardo, L., Marx, M. A., Richter, D. and Tanis, S. P. (2011) Discovery of Novel, Potent, and Selective Inhibitors of 3-Phosphoinositide-Dependent Kinase (PDK1). *J. Med. Chem.*, **54**, 8490 - 8500; (c) Osborne, J. D., Matthews, T. P., McHardy, T., A., Proisy, N., Cheung, K. -M. J., Lainchbury, M., Brown, N., Walton, M. I., Eve, P. D., Boxall, K. and Katherine, J. (2016) Multiparameter Lead Optimization to Give an Oral Checkpoint Kinase 1 (CHK1) Inhibitor Clinical Candidate: (R)-5-((4-((Morpholin-2-ylmethyl)amino)-5-(trifluoromethyl) pyridin-2-yl)amino)pyrazine-2-carbonitrile (CCT 245737) *J. Med. Chem.*, **59**, 5221 - 5237. (d) Berg, S., Bergh, M., Hellberg, S., Hoegdin, K., Alfredsson, Y. L., Soederman, P., von Berg, S., Weigelt, T., Ormoe, M. and Xue, Y. (2012) Discovery of Novel Potent and Highly Selective Glycogen Synthase Kinase-3β (GSK3β) Inhibitors for Alzheimer's Disease: Design, Synthesis, and Characterization of Pyrazines. *J. Med. Chem*., **55**, 9107 – 9119. e) Rahmani, R., Ban, K., Jones, A. J., Ferrins, L., Ganame, D., Sykes, M. L., Avery, V. M., White, K. L., Ryan, E. and Kaiser, M. (2015) 6-Arylpyrazine-2-carboxamides: A New Core for Trypanosoma brucei Inhibitors. *J. Med. Chem.*, **58**, 6753 - 6765. (f) Younis, Y., Douelle, F., Cabrera, D. G., Manach, C. L., Nchinda, A. T., Paquet, T., Street, L. J., White, K. L., Zabiulla, M. K., Joseph, J. T., Bashyam, S., Waterson, D., Witty, M. J., Wittlin, S., Charman, S. A. and Chibale, K. (2013) Structure–Activity-Relationship Studies around the 2-Amino Group and Pyridine Core of Antimalarial 3,5-Diarylaminopyridines Lead to a Novel Series of Pyrazine Analogues with Oral in Vivo Activity. *J. Med. Chem*., **56,** 8860 - 8871.

4. World Health Organization (2018) Avenue Appia, Geneva, **20**, 1211.

5. Anand, P., Kunnumakara, A. B., Sundaram, C., Harikumar, K. B., Tharakan, S. T., Lai, O. S., Sung, B. and Aggarwal, B. B. (2008) Cancer is a Preventable Disease that Requires Major Lifestyle Changes. *Pharma. Res.*, **25**, 2097-2116.

6. Dhingra, A. K., Chopra, B., Dass, R. and, Mittal, S. K. (2015). An update on Anti-inflammatory Compounds. *Anti-inflamm. Anti-allergy Agents in Med. Chem*., **14**, 81-97.

7. Lucas, S. M., Rothwell, N. J. and Gibson, R. M. (2006) The role of inflammation in CNS injury and disease. *Br. J. Pharmacol*., **147**, S232-S240.

8. Coussens, L. M. and Werb, Z. (2002) Inflammation and cancer. *Nature*, **420**, 860-867.

9. Abou-Raya, A. and Abou-Raya, S. (2006) Inflammation: A pivotal link between autoimmune diseases and atherosclerosis. *Autoimmun. Rev.*, **5**, 331-337.

10. Ridker, P. M., Cushman, M., Stampfer, M. J., Tracy, R. P. and Hennekens, C. H. (1997) Inflammation, Aspirin, and the Risk of Cardiovascular Disease in Apparently Healthy Men. *N. Engl. J. Med*., **336**, 973-979.

11. Teixeira, B. C., Lopes, A. L., Macedo, R. C. O., Correa, C. S., Ramis, T. R., Ribeiro, J. L. and Reischak-Oliveira, A. J. (2014) Inflammatory markers, endothelial function and cardiovascular risk. *J. Vasc. Bras.*, **13**, 108-115.

12. Stanisic, M., Lyngstadaas, S. P., Pripp, A. H., Aasen, A. O., Lindegaard, K. F., Ivanovic, J., Ilstad, E., Konglund, A., Sandell, T., Ellingsen, O. and Saehle, T. (2012) Chemokines as markers of local inflammation and angiogenesis in patients with chronic subdural hematoma: a prospective study. *Acta. Neurochir*., **154**, 113-120.

13. Sanchez-Muñoz, F., Dominguez-Lopez, A., Yamamoto-Furusho, J. K. (2008) Role of cytokines in inflammatory bowel disease. *World journal of gastroenterology*, **14**, 4280-4288.

14. Zelová, H., Hošek, J. (2013) TNF-α signalling and inflammation: interactions between old acquaintances. *Inflamm. Res.*, **62,** 641–651.

15. Papadakis, K. A. and Targan, S. R. (2006) The role of chemokines and chemokine receptors in mucosal inflammation. *Inflamm. Bowel. Dis.*, **6**, 303–313.

16. Rus, F. G., Niculescu, F. and Vlaicu, R. (1991) Tumor necrosis factor-alpha in human arterial wall with atherosclerosis. *Atherosclerosis*, **89**, 247–254.

17. Newton, R. C. and Decicco, C. P. (1999) Therapeutic Potential and Strategies for Inhibiting Tumor Necrosis Factor-α. *J. Med. Chem.*, **42**, 2295–2314.

18. Milliani, F. L., Nielsen, O. H., Andersen, P. S. and Giradin, S. E. (2007) Chronic inflammation: importance of NOD2 and NALP3 in interleukin-1β generation. *Clin & Exp Immunol*, **147**, 227-235.

19. Young-Dae, G., Mi-Sook, D., Sang-Bum, L., Nayeon, K., Mi-Seon, B. and Nam-Sook, K. (2011) A novel 3-arylethynyl-substituted pyrido[2,3,-b]pyrazine derivatives and pharmacophore model as Wnt2/β-catenin pathway inhibitors in non-small-cell lung cancer cell lines. *Bioorg. Med.Chem.*, **19**, 5639-5647.

20. Sahina, M. F., Badıçoglu, B., Gökçe, M., Küpeli, E. and Yeşilada, E. (2004) Synthesis and Analgesic and Antiinflammatory Activity of Methyl 6-Substituted-3(2H)-pyridazinone-2-ylacetate Derivatives. *Arch. Pharm. Med. Chem*., **337,** 445-452.

21. Crowley, P. J., Lamberth, C., Müller, U., Wendeborn, S., Nebel, K., Williams, J., Sageot, O., Carter, N., Mathie, T., Kempf, H. J., Godwin, J., Schneiter, P. and Dobler, M. R. (2010) Synthesis and fungicidal activity of tubulin polymerisation promoters. Part 1: pyrido[2,3-b]pyrazines. *Pest Manag Sci.*, **66**, 178-185.

22. Castellanos, J. M., Hernández, K. R., Gómez-Flores, N. S., Rodas-Suárez, O. R. and Peralta-Cruz, J. (2012) Microwave-assisted Solvent-free Synthesis and in Vitro Antibacterial Screening of Quinoxalines and Pyrido[2,3,b]pyrazines. *Molecules.*, **17**, 5164-5176.

23. Temple, C. and Rener, G, A. (1990) Potential antimitotic agents. Synthesis of some ethyl benzopyrazin-7-ylcarbamates, ethyl pyrido[3,4-b]pyrazin-7-ylcarbamates, and ethyl pyrido[3,4-e]-as-triazin-7-ylcarbamates. *J. Med. Chem*., **33**, 3044-3050.

24. Zhang, X. Z., Wang, J. X., Sun, Y. J. and Zhan, H. W. (2010) Synthesis of quinoxaline derivatives catalyzed by PEG-400. *Chin. Chem. Lett.*, **21**, 395–398.

25. Guo, W. X., Jin, H. L., Chen, J. X., Chen, F., Ding, J. C. and Wu, H. Y. (2009) An efficient catalyst-free protocol for the synthesis of quinoxaline derivatives under ultrasound irradiation. *J. Braz. Chem. Soc*., **20**, 1674-1679.

26. Zhou, W. J., Zhang, X., Sun, X. B., Wang, B., Wang, J. X. and Bai, L. (2014) Microwave-assisted synthesis of quinoxaline derivatives using glycerol as a green solvent. *Russ. Chem. Bull*., **62**, 1244-1247.

27. Vaghei, R. G. and Hajinazari, S. (2013) Poly(N,N ′-dibromo-N-ethyl-benzene-1,3-disulphonamide) and N,N,N ′,N ′-tetrabromobenzene-1,3-disulphonamide as novel catalysts for synthesis of quinoxaline derivatives. *J. Chem. Sci*., **125**, 353–358.

28. Robinson, R. S. and Taylo, R. J. K. (2005) Quinoxaline Synthesis from α-Hydroxy Ketones via a Tandem Oxidation Process Using Catalysed Aerobic Oxidation. *Synlett.*, **6**, 1003–1005.

29. Hasaninejad, A., Zare, A., Reza, M., Izadeh, M. and Shekouhy, M. (2010) Lithium bromide as an efficient, green, and inexpensive catalyst for the synthesis of quinoxaline derivatives at room temperature. *Gree. Chem. Lett. and Reviews*, **3**, 143-148.

30. Huang, T., Wang, R., Shi, L., Lu, X. (2008) Montmorillonite K-10: An efficient and reusable catalyst for the synthesis of quinoxaline derivatives in water. *Cataly. Commu*., **9**, 1143–1147.

31. Hazarika, P., Gogoi, P. and Konwar, D. (2007) Efficient and Green Method for the Synthesis of 1,5-Benzodiazepine and Quinoxaline Derivatives in Water. *Synth. Commu*., **37**, 3447–3454.

32. Heravi, M. M., Tehrani, M. H., Bakhtiari, K., Oskooie, H. A. (2007) Zn[(l)proline]: A powerful catalyst for the very fast synthesis of quinoxaline derivatives at room temperature. *Cataly. Commu.*, **8**, 1341–1344.

33. Cai, J. J., Zou, J. P., Pan, X. Q. and Zhang, W. (2008) Gallium(III) triflate-catalyzed synthesis of quinoxaline derivatives. *Tetrahedron Lett.*, **49,** 7386-7390.

34. Das, B., Katta, B. V., Kanaparthy, S. and Anjoy, M. (2007) An efficient and convenient protocol for the synthesis of quinoxalines and dihydropyrazines via cyclization–oxidation processes using HClO4·SiO2 as a heterogeneous recyclable catalyst. *Tetrahedron Lett.*, **48**, 5371-5374.

35. Madhav, B., Murthy, S. N., Reddy, V. P., Rao, K. R. and Nageshwar, Y. V. D. (2009) Biomimetic synthesis of quinoxalines in water. *Tetrahedron Lett*., **50**, 6025-6028.

36. Rao, K. T. V., Sai Prasad, P. S., and Lingaiah, N. (2009) Iron exchanged molybdophosphoric acid as an efficient heterogeneous catalyst for the synthesis of quinoxalines. *J. Mol. Catal. A-Chem*., **312**, 65-69.

37. Krishnakumar, B. and Swaminathan, M. (2010) A recyclable and highly effective sulfated TiO2-P25 for the synthesis of quinoxaline and dipyridophenazine derivatives at room temperature. *J. Organomet. Chem.*, **695**, 2572-2577.

38. Katkar, S. S., Mohite, P. H., Gadekar, L. S., Arbad, B. R. and Lande, M. K. (2010) ZnO-beta zeolite mediated simple and efficient method for the one-pot synthesis of quinoxaline derivatives at room temperature. *Cent. Eur. J. Chem*., **8**, 320-325.

39. Darbari, H. R., Aghapoor, K., Mohsenzadeh, F., Taala, F., Asadollahnejad, N. and Badiei, A. (2009) Silica-Supported Antimony(III) Chloride as Highly Effective and Reusable Heterogeneous Catalyst for the Synthesis of Quinoxalines. *Catal. Lett.*, **133**, 84-89.